Catalysis Today 182 (2012) 3–11

Contents lists available at SciVerse ScienceDirect

Catalysis Today

journal homepage: www.elsevier.com/locate/cattod

# New insights into the methanol oxidation mechanism over $Au/CeO_2$ catalyst through complementary kinetic and FTIR *operando* SSITKA approaches

P. Bazin, S. Thomas, O. Marie*, M. Daturi

*Laboratoire Catalyse et Spectrochimie, ENSICAEN, Université de Caen, CNRS, 6 Bd Maréchal Juin, F-14050 Caen, France*

ARTICLE INFO

*Article history:*
Received 10 June 2011
Received in revised form 4 October 2011
Accepted 5 October 2011
Available online 8 November 2011

*Keywords:*
Methanol oxidation
Au nanoparticles
IR spectroscopy
Reaction mechanism
SSITKA

ABSTRACT

The mechanism of methanol full oxidation over $Au/CeO_2$ in the low temperature range has been clarified combining FT-IR spectroscopic results with kinetic calculations. A clear thermal effect of the infrared beam on the catalytic reaction was remarked and quantified. A global mechanistic model was proposed, providing the reaction order, the kinetic constants and the activation energy for the process, as well as valuable information on selected elemental steps. SSITKA experiments gave additional evidences on the formate decomposition as the rate determining step (RDS) of the reaction and proved the strict correlation between formate decomposition and $CO_2$ yield, at different temperatures, further validating the kinetic model and differentiating the activation energy of the RDS from the apparent activation energy of the process as a whole.



## 1. Introduction

Increasing concerns about the quality of life and the number of environmental hazards which can constitute a danger for the human health incite scientists to found alternative ways to control the quality of air. Besides the efforts in progress to abate car exhaust and industry emissions, a real problem has been verified concerning confined environments where people spend the majority of their time: house interiors, offices, vehicle cockpits, etc. . . . Furniture's, carpets and paintings are a source of dangerous VOC [1–3], while the majority of filters for air admission in the cars are almost ineffective, making the vehicle cockpit one of the most dangerous place for pollutant concentration [4]. For these reasons, new enhanced media for air purification are under current development. Among them, the tendency is to favor renewable systems, intended to be regenerated, decreasing therefore the raw material waste and the recycling costs. Another, greener concept consists in developing catalytic devices able to abate VOC at the minimum energetic expense. In this frame, gold-based materials represent a unique class of catalysts able to effectively oxidize different harmful compounds at room temperature (and even below) without any energetic supply. The capability of gold nanoparticles to oxidize CO is well known [5–7] and recently, the performances of $Au/CeO_2$ on the oxidation of more complex, organic compounds were investigated, showing that this material is able to eliminate target molecules such as methanol at room temperature. Regarding the mechanism for alcohol oxidation over $Au/CeO_2$ catalyst, a study dealing with ethanol conversion in the 373–1073 K range reports, through TPD and IR spectroscopy, the formation of ethoxide and CO adsorbed species [8]. While ethanol has a C–C bond and therefore its chemistry is different from that of methanol some analogies can be drawn in particular those related to alkoxide (methoxy) and CO species. A complete reaction mechanism was indeed described for room temperature methanol oxidation [9], showing the role of surface sites towards the adsorption of reactive agents and the formation of intermediates till the final products ($CO_2$ and water). Nevertheless, some details in selected elemental steps remained to be clarified, notably concerning the nature of the intermediate species involved in the rate determining step of the reaction. For these reasons, additional investigations were performed using a SSITKA approach combined with infrared (IR) *operando* analysis system. The obtained data were processed by a kinetic model and these new, complementary results will be the object of the present report.

## 2. Experimental

The $Au/CeO_2$ sample synthesis and its characteristics are reported in details within reference [9]. The main physico-chemical properties are the following: specific surface area = 180 $m^2\ g^{-1}$, Au content = 1 wt% and gold particle size < 3 nm.

A scheme of the SSITKA *operando* system which was used for this study is provided in Fig. 1; it is composed of four main parts: the infrared spectrometer, the IR reactor-cell, the gas flow set-up

* Corresponding author.
*E-mail address:* olivier.marie@ensicaen.fr (O. Marie).

0920-5861/$ – see front matter © 2011 Elsevier B.V. All rights reserved.
doi:10.1016/j.cattod.2011.10.001

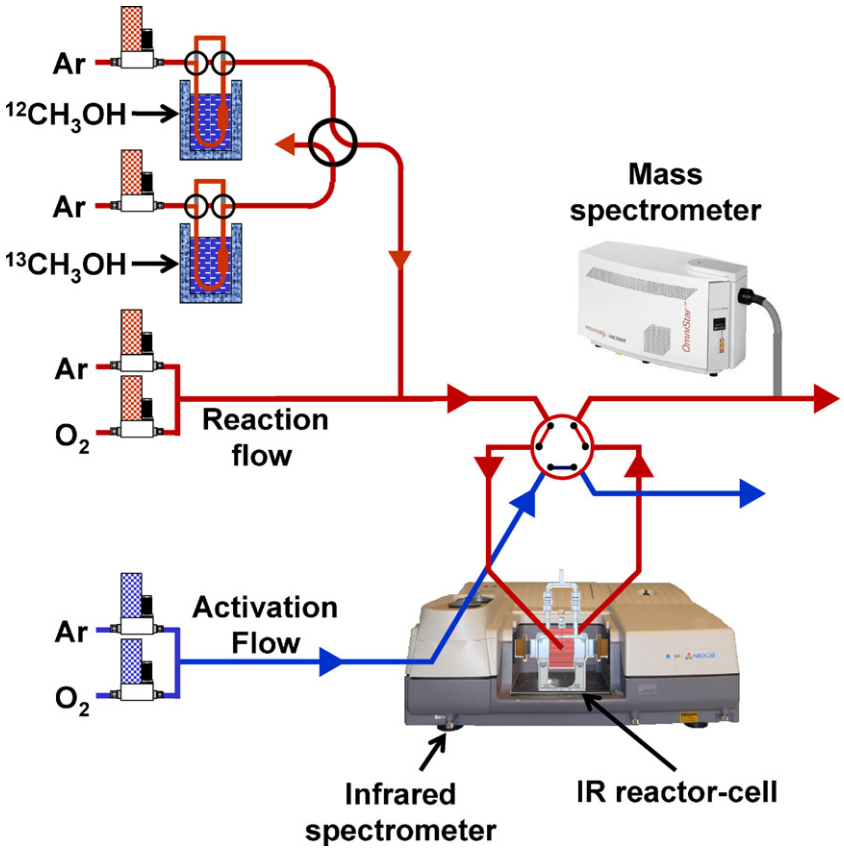


**Fig. 1.** Scheme of the SSITKA equipment used for this investigation.

and the exhaust gas analyzers. The cell is connected to the *operando* gas-system including mass flow controllers for the introduction of gases into the lines. The two gas mixtures, so called the activation and the reaction flow, can be prepared and sent independently to the reactor cell. The system allows investigating the exhaust gases (reactive and/or reaction products) by a Quadrupole Mass Spectrometer (Pfeiffer Omnistar GSD 301), while complementary information on the gas phase can be gained by IR spectroscopy (which was not used in the present study) through a gas micro-cell. Regarding the catalyst under duty, IR spectra (64 scans per spectrum) were collected at a time resolution of 1 spectrum per minute with a Thermo Scientific Nicolet 6700 spectrometer, equipped with a MCT detector. More details can be found in the following references for both the IR *operando* system [10,11] and the so-called *Sandwich* IR reactor-cell [12]. For this specific study, the system was implemented by two saturators located in the same thermostated bath (at exactly the same temperature), in order to send, via a 4 ways valve, a fixed concentration of vaporized methanol, either in its natural form or in the 99.0% $^{13}C$ enriched form, provided by Cambridge Isotope Laboratories. The flow conditions were as follows: 700 ppm of $CH_3OH$, 20% of oxygen diluted in Argon at a constant gas hourly space velocity of 60,000 $h^{-1}$. The reaction was studied within the temperature range of [298–343 K].

## 3. Results and discussion

### 3.1. Thermal effect of the IR beam on the catalytic activity

In a previous study [9], a mechanism for low temperatures methanol oxidation on a nanostructured $Au/CeO_2$ catalyst was proposed using *operando* FTIR spectroscopy of the catalytic surface coupled with the gas phase analysis, using both mass spectrometry and complementary IR spectroscopy. The gas phase analysis by IR was specifically applied to discard the presence of any partially oxidized molecules such as formaldehyde or CO whose formation would not satisfy the harmlessness principle of the target molecule (methanol in the present case) removal. However, our IR *operando* system is equipped with one single IR source and thus it was necessary to alternately send the IR beam to the catalyst or to the gas phase analysis through a mobile mirror. In these conditions of analysis, periodic phenomena were observed during the reaction (Fig. 2). The reasons for that could be different: CO oxidation is often affected by kinetic oscillations [13,14];

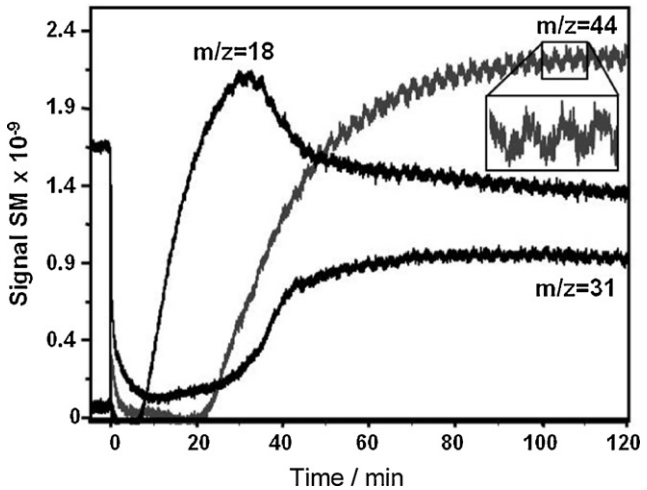


**Fig. 2.** Zoom on the MS profiles of the main species involved during methanol oxidation over $Au/CeO_2$ at 323 K, highlighting the presence of periodic phenomena.

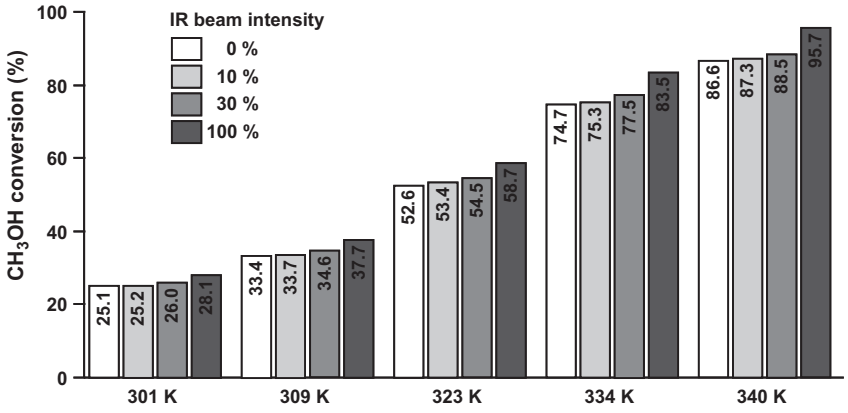


**Fig. 3.** $CH_3OH$ conversion to $CO_2$ over $Au/CeO_2$. The histogram plot illustrates the IR beam intensity effect on the conversion at a given temperature.

mass flow controller instability or analyzer defects could also been invoked. In the reality, such oscillatory phenomena were not random and a detailed analysis indicates that gas phase methanol evolution is in phase opposition with both water and $CO_2$ evolution as expected for any oxidation reaction. Furthermore, the oscillation period strangely correlated with the infrared beam scanning duration. As gold nanoparticles are active already at room temperature and even below, the investigated reaction is highly temperature sensitive and, therefore, even a slight change in the temperature may influence the reactivity. The hypothesis of a photocatalytic activation of the ceria by IR irradiation was disregarded, as, to our best knowledge, no literature data report such a phenomenon. On another hand, when different grids (70% and 90% of occultation) were placed between the IR beam and the cell windows in order to attenuate the IR light intensity received by the catalyst, noticeable effects were detected. Fig. 3 provides clear evidences that for each fixed temperature of the IR reactor cell, the methanol conversion rises with the amount of IR beam received by the catalyst, indeed. The oscillations observed when analyzing alternately the catalysts surface and the gas phase by IR are thus clearly due to the periodic infrared beam heating of catalyst surface, equivalent to a thermal effect of +3.5 K.

### 3.2. $CH_3OH$ partial reaction order and apparent activation energy

An estimation of the reactant partial order of reaction and of the apparent activation energy was attempted from the above data. Assuming that our IR reactor cell behaves as a plug flow reactor (PFR) operating in the integral mode (conversion between 25 and 100%), the starting equation for a kinetic processing of the data is the expression of the local reaction rate per unit mass of catalyst $r_m$:

$$r_m = F_{CH_3OH}\frac{df}{dw_c}$$

where $dw_c$ is the weight of an infinitesimal catalyst amount, $F_{CH_3OH}$ is the methanol molar flow at the inlet and $df$ is the methanol local conversion variation. In the general case, this expression is not an explicit mathematical relation since $r_m$ most often depends on the conversion. The most difficult task then consists in the determination of the mathematical expression making the link between $r_m$ and $f$ [15]. However, in the frame of methanol transformation over noble metal supported onto metal oxides, Kapoor et al. reported a linear evolution in a broad range of conversion when plotting $\mathrm{Ln}(f) = f(1/T)$ [16]. From this plot, the apparent activation energy for the selective decomposition of methanol into CO and $H_2$ over $Pd/CeO_2$ was estimated [16]. It is worth noting that such an evolution implies that the local reaction rate can be considered independent from the conversion, even for an integral PFR. After integration over the whole catalyst weight, the approximate algorithm describing the process is thus sharply simplified as: $r_m = F_{CH_3OH}f/w_c$, where $f$ corresponds to the observed conversion at the catalyst outlet (which makes $r_m$ also corresponding to the global activity of the catalyst in mol $s^{-1}$ $g^{-1}$). On another hand, $r_m$ can be expressed as the product of several constants, among which a kinetic rate constant satisfying the Arrhenius relation. As a result, we get ($A$ being a global constant and $E^a_{app}$ being the apparent activation energy): $Ae^{-E^a_{app}/RT} = F_{CH_3OH}f/w_c$ which fully justify the observed linear plot. Similarly to what proposed by Kapoor et al., Fig. 4A thus plots the overall data obtained previously (Fig. 3), in the presence or not of an IR beam irradiation of the surface. The $1/T$ variable in $x$-coordinate was calculated from the temperature value imposed to the reactor cell via the heating regulation system and obviously all the data obtained in presence of the IR beam perfectly follow a linear evolution assuming that 100% of the IR beam induces a local heating effect corresponding to an increment of temperature equal to 3.5 K (see Fig. 4B). The slope calculated from Fig. 4B allowed estimating an apparent activation energy for the methanol catalytic full oxidation over $Au/CeO_2$ of $E^a_{app} = 27.6\ \mathrm{kJmol^{-1}}$. This value is very similar to that calculated in our previous paper [9] and much lower than those previously reported for the selective decomposition of methanol over $Pd/CeO_2$, i.e. $E^a_{app} = 55–90\ \mathrm{kJmol^{-1}}$, which were associated to the methoxy decomposition into CO and $H_2$ as the rate determining step [16,17]. As already remarked, such a low activation energy is a proof of the excellent performances of this catalyst. Finally, it is worth emphasizing, as a conclusion, that the observed perfect linear plot of $\mathrm{Ln}(f)$ versus $1/T$ implies that the rate equation does not depend on the methanol conversion and thus that $CH_3OH$ partial order of reaction is zero.

### 3.3. A kinetic model for the reaction

Our methodology based on time resolved simultaneous analysis of adsorbed and gaseous species allowed evaluating some catalytic reaction parameters of the investigated material towards $CO_2$ production and identifying a series of steps in the oxidation pathway. In particular, it was found [9] that:

i) methanol adsorbs dissociatively on the ceria surface forming methoxys;
ii) linearly and bridged adsorbed methoxys behaves as intermediates, transforming then into formates (only in presence of gold in the considered low temperature range), while other types of methoxy species are spectators;

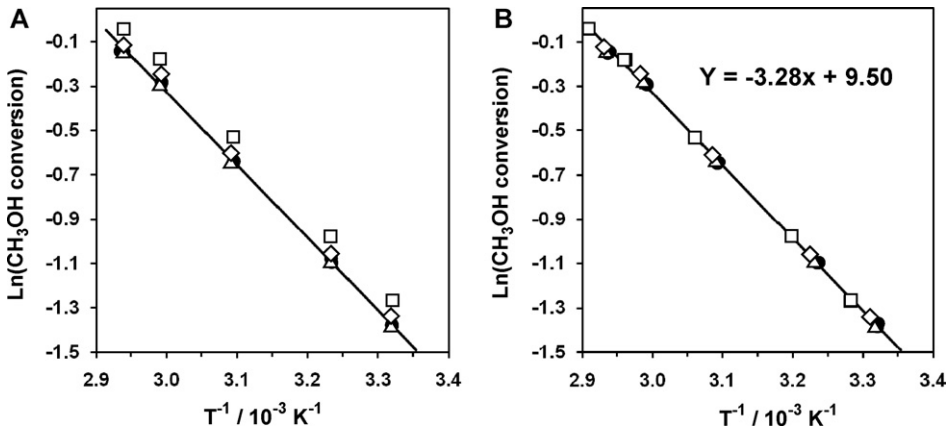


**Fig. 4.** Ln($CH_3OH$ conversion) versus $1/T$ for IR beam intensity of: (○) 0%, (△) 10%, (◊) 30% and (□) 100%. (A) Uncorrected data. (B) Data corrected in order to take into account the IR beam heating effect.

iii) formates, whose transformation was found – considering their thermal behavior – to be the rate determining step (RDS) for the reaction, decompose into CO and OH species;
iv) this decomposition only takes place in the neighborhoods of the gold nanoparticles (in a zone identified as an "active perimeter"), where gold oxidizes adsorbed CO to $CO_2$.

For modeling simplicity seek, the active perimeter (whose real nature is still object of discussions and investigations) was here limited to the interface between gold nanoparticles and the ceria support even though it may extend through oxygen spill-over and reverse spill-over domains. Moreover, linearly adsorbed methoxys were taken into account as representative of the main methoxy intermediate species. Finally, in order to take into account the gold involvement for methoxys conversion into formates, we invoke [*Ce_HCOO_Au*] formate species at the gold/ceria interface while no clear IR signature of such a species could be discriminated from those typical for formates on ceria alone. The previous reaction model can thus be represented by the following set of five successive elemental steps.

$$*Au + O_2 \rightleftarrows *Au\_O_2 \qquad (K_1)$$
$$*Ce\_OH + CH_3OH \rightleftarrows *Ce\_CH_3O + H_2O \qquad (K_2)$$
$$*Ce\_CH_3O + *Au\_O_2 \rightleftarrows *Ce\_HCOO\_Au* + H_2O \qquad (K_3)$$
$$*Ce\_HCOO\_Au* \rightarrow *Au\_CO + *Ce\_OH \qquad (k_4)$$
$$*Au\_CO + \tfrac{1}{2}\,O_2 \rightleftarrows *Au + CO_2 \qquad (K_5)$$
$$CH_3OH + 3/2\,O_2 \Longrightarrow CO_2 + 2\,H_2O$$

where *Au and *Ce are superficial active sites, $K_1$, $K_2$ are adsorption equilibrium constants and $K_3$, $K_5$ are equilibrium constants for steps 3 and 5 respectively. Assuming the formate decomposition as the non reversible RDS, in presence of oxygen excess, the rate can be defined as: $r_m = F_{CH_3OH}\, df/dw_c = k_4\,[*Ce\_HCOO\_Au*]$ where $k_4$ stands for the step 4 kinetic rate constant.

Adsorption steps 1 and 2 are quasi-equilibrated, so

$$K_1 = \frac{[*Au\_O_2]}{[*Au]P_{O_2}} \tag{1}$$

and

$$K_2 = \frac{[*Ce\_CH_3O]P_{H_2O}}{[*Ce\_OH]P_{CH_3OH}} \tag{2}$$

Reactions (3) and (5) are also quasi-equilibrated, so

$$K_3 = \frac{[*Ce\_HCOO\_Au*]P_{H_2O}}{[*Au\_O_2][*Ce\_CH_3O]} \tag{3}$$

and

$$K_5 = \frac{[*Au]P_{CO_2}}{[*Au\_CO]{P_{O_2}}^{1/2}} \tag{5}$$

Solving Eqs. (1) and (2) for [*Au_$O_2$] and [*Ce_$CH_3O$] respectively, substituting these values into Eq. (3) and rearranging it gives

$$[*Ce\_HCOO\_Au*] = K_1K_2K_3P_{O_2}P_{CH_3OH}P_{H_2O}^{-2}[*Au][*Ce\_OH] \tag{6}$$

Previous *operando* studies have indicated that methoxy species are the most abundant reaction intermediates (MARI) onto ceria [9], moreover the cerium cations onto the surface are either occupied by methoxys, or hydroxylated. Thus, labeling $L_{Ce}$ the total superficial concentration of Ce cation, one gets:

$$L_{Ce} = [*Ce\_OH] + [*Ce\_CH_3O] \tag{7}$$

which gives

$$[*Ce\_OH] = \frac{L_{Ce}}{1 + K_2P_{CH_3OH}/P_{H_2O}} \tag{8}$$

Furthermore, the study of methanol adsorption over the bare ceria support showed, under similar flow and temperature conditions, that the steady state methoxys surface coverage level was close to unity [9]. In presence of gold, adsorbed formates appeared at the expense of methoxys but the [*Ce_$CH_3O$]/[*Ce_OH] ratio remained $\gg$1. Consequently one may assume from both the *operando* catalyst surface observation and Eq. (2), that under reaction conditions $1 \ll K_2P_{CH_3OH}/P_{H_2O}$.

We thus obtain after simplification of (8) and substitution in Eq. (6):

$$[*Ce\_HCOO\_Au*] = K_1K_3P_{O_2}P_{H_2O}^{-1}L_{Ce}[*Au] \tag{9}$$

Considering now the gold active sites and indicating by $L_{Au}$ the total superficial concentration of Au sites (similarly to what made above for cerium), one can consider

$$L_{Au} = [*Au] + [*Au\_O_2] + [*Ce\_HCOO\_Au*] + [*Au\_CO] \tag{10}$$

CO adsorbed onto gold was detected under reaction condition but it gave a very weak IR signal; the molar absorption coefficient of CO on gold nanoparticles is up to now unknown, but considering that CO oxidation on Au sites is a fast step, carbonyl concentration can be neglected in a first approximation. On another hand, although formates were easily detected, the impossibility by IR to observe adsorbed $O_2$ imposes to consider two possible MARI's onto gold.

* First hypothesis: $MARI_{Au} = [^*Au\_O_2]$

$$L_{Au} = [*Au] + [*Au\_O_2] \quad (11)$$

which combined with Eq. (1) gives

$$[Au*] = \frac{L_{Au}}{1 + K_1 P_{O_2}} \quad (12)$$

After reinjection in Eq. (9), one obtains

$$[*Ce\_HCOO\_Au*] = K_1 K_3 P_{O_2} P_{H_2O}^{-1} L_{Ce} \frac{L_{Au}}{1 + K_1 P_{O_2}} \text{ and thus} \quad (13)$$

$$r_m = k_4 K_1 K_3 P_{O_2} P_{H_2O}^{-1} L_{Ce} L_{Au} \frac{1}{1 + K_1 P_{O_2}} = k_{app} \frac{P_{O_2} P_{H_2O}^{-1}}{1 + K_1 P_{O_2}} \quad (14)$$

Considering $[^*Au\_O_2]$ as the MARI onto gold, one cannot here distinguish whether the coverage of gold by oxygen is high ($1 \ll K_1 P_{O_2}$) or low enough to satisfy ($1 \gg K_1 P_{O_2}$). In the former case, the apparent activation energy, deduced from the gas phase data, can be approximated by $E^a_{app} = E^a_{RDS} + \Delta H_3$ while in the latter case the $O_2$ adsorption enthalpy $\Delta H_1$ should be added. Nevertheless, in both cases, the apparent activation energy will be lower than the activation energy required for the rate determining step, since both adsorption (step 1) and oxidation (step 3) are exothermic reactions.

* Second hypothesis: $MARI_{Au} = [^*Ce\_HCOO\_Au^*]$

$$L_{Au} = [*Au] + [*Ce\_HCOO\_Au*] \quad (15)$$

which combined with Eqs. (1), (2), (3) and (8) gives

$$[Au*] = \frac{L_{Au}}{1 + K_1 K_3 P_{O_2} P_{H_2O}^{-1} L_{Ce}} \quad (16)$$

After reinjection in Eq. (9), it results

$$[*Ce\_HCOO\_Au*] = K_1 K_3 P_{O_2} P_{H_2O}^{-1} L_{Ce} \frac{L_{Au}}{1 + K_1 K_3 P_{O_2} P_{H_2O}^{-1} L_{Ce}}$$

which finally gives (17)

$$r_m = k_4 K_1 K_3 P_{O_2} P_{H_2O}^{-1} L_{Ce} \frac{L_{Au}}{1 + K_1 K_3 P_{O_2} P_{H_2O}^{-1} L_{Ce}}$$

that can be approximated into (18)

$$r_m = k_4 L_{Au} \quad (19)$$

or

$$r_m = k_4 K_1 K_3 P_{O_2} P_{H_2O}^{-1} L_{Ce} L_{Au} = k_{app} P_{O_2} P_{H_2O}^{-1} \quad (20)$$

depending of the value of $K_1 K_3 P_{O_2} P_{H_2O}^{-1} L_{Ce}$ compared to unity and thus depending on the extent of gold coverage by formates.

To summarize, it should be emphasized that considering the methoxy as the MARI onto ceria and taking into account the high methoxy coverage level in reaction conditions, lead to a good agreement with the zero reaction order observed for methanol and this whatever the hypothesis regarding the MARI onto gold (see Eqs. (14), (19) and (20)). Furthermore, the measured apparent activation energy will be lower than the activation energy relative to the RDS except if $[^*Ce\_HCOO\_Au^*]$ is the MARI onto gold and $K_1 K_3 P_{O_2} P_{H_2O}^{-1} L_{Ce} \gg 1$ where $E^a_{app} \cong E^a_{RDS}$ is expected.

### 3.4. A complementary study by SSITKA

#### 3.4.1. Analysis of the reaction step sequence

Although the description of the mechanism appears complete, some points still need clarification. In particular, it will be interesting to observe (besides having calculated) the formate decomposition as the slow reaction step and to quantify some kinetic parameters leading the catalytic reaction. For these reasons our investigation was completed by SSITKA experiments using isotopic labeled methanol and by subsequent kinetic processing of the data.

As already pointed out, it is often better making abstraction of the *operando* conditions to identify reaction intermediates and active sites [18–20]: transient conditions may be more informative evidencing species having short lifetime and low concentration, intrinsically. But this requires a conceptual extrapolation, assuming that the results found out of the reaction conditions also apply to the real case. To circumvent the problem, the use of the SSITKA methodology allows obtaining transient conditions while remaining under the required chemical and kinetic steady state environment for a given reaction [21,22].

In the present case, the SSITKA experiment was performed using two reaction flows in our *operando* system, each of them equipped with a saturator containing either natural methanol of $^{13}C$ enriched one (Fig. 1). A four ways valve permits to switch instantaneously from a flow to another, whose concentrations have been calibrated. Therefore, the reaction behaves chemically identical in both cases. A $^{13}C$-substituted methanol containing flow was sent first to the sample. Regular methoxys and formates infrared bands are visible on the surface under steady-state conditions, presenting the expected isotopic shift [23] (Fig. 5). It is worth noting that under similar temperature and flow conditions over the bare ceria support, traces of molecularly adsorbed methanol were detected. Such non dissociative $^{12}CH_3OH$ adsorption leads to a shoulder at 1028 $cm^{-1}$ rendering the type II and II′ methoxys $\nu$(CO) bands highly dissymmetric [9]. In the present study, Fig. 5 upper part right hand corner shows symmetric $\nu$(CO) bands with no shoulder at 1009 $cm^{-1}$ where molecularly adsorbed $^{13}CH_3OH$ would be expected. Starting from the chemical steady state ($t = 0$), the reaction flow was switched to the natural methanol containing flow and consequently both the bands of adsorbed methoxy and formates species progressively replaced the previously formed species, giving rise to several isobestic points. It is worth noting that when the new equilibrium state of the surface was reached, the entirety of $^{13}C$ previously adsorbed species disappeared. This reveals that, if present, the spectator species are not poisoning active sites upon strong interaction. Furthermore, focusing on the adsorbed methoxy region, the replacement rate of type I and II intermediate species or of type II′ spectator species cannot be discriminated. This confirms that whatever the adsorption site, the methanol dissociative adsorption is a fast step of the reaction. The same observation can be made for the formate species, whose homogeneous broad band evolution does not allow the discrimination of any specific component from the rest. Comparing the first five spectra after the switch was made, it is moreover obvious that the methoxy replacement rate is much faster than that of formates, thus confirming that the formate formation takes place when the methoxy coverage level is high. Finally, the inlets on Fig. 5 represent the initial equilibrium intensities of bands typical for both methoxys (1000–1100 $cm^{-1}$) and formates (1300–1400 $cm^{-1}$) at increasing reaction temperatures. When the temperature increases, the amount of adsorbed formates rises at the expense of the amount of adsorbed methoxys. Consequently, one can conclude that when the methanol oxidation steady state is reached, the ceria surface is almost fully covered and that the formate formation proceeds from methoxy oxidation. It was from the similar observation of a higher amount of adsorbed formates at higher temperatures that formate decomposition was deduced as the rate determining step in our previous study [9].

#### 3.4.2. Evidencing the rate determining step

The main, characteristic bands of the methoxy ($^{12}C$: 1101 $cm^{-1}$ and $^{13}C$: 1082 $cm^{-1}$) and formate ($^{12}C$: 1380 $cm^{-1}$ and $^{13}C$:

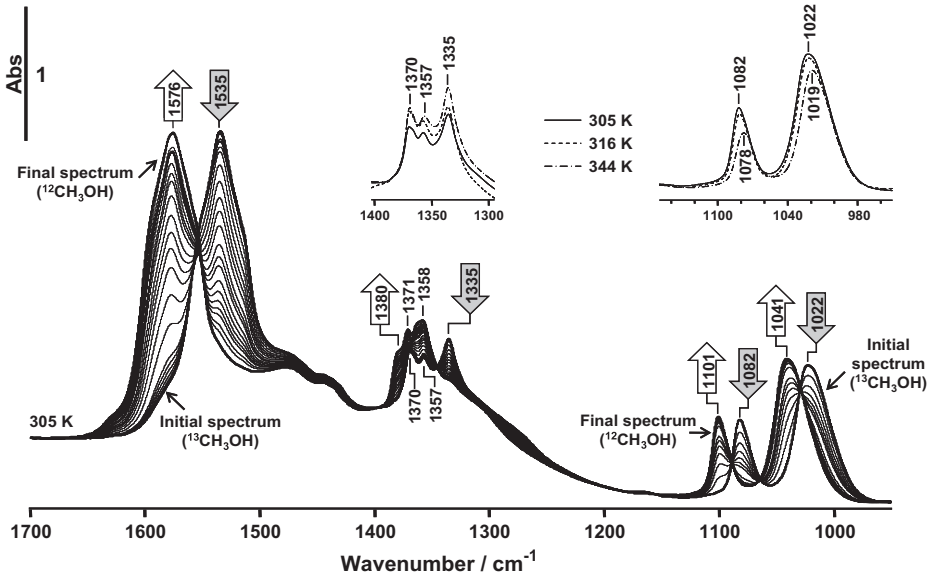


**Fig. 5.** IR spectra of $Au/CeO_2$ recorded at 305 K during a SSITKA experiment for which an initial flow made of 700 ppm of $^{13}CH_3OH$, 20% of oxygen diluted in Ar (total flow = 20 $cm^3$ $min^{-1}$) was switched to a similar non labeled ($^{12}CH_3OH$) flow. The inserts illustrate the initial band intensities for typical species at various reaction temperatures (corrected to take into account the influence of the IR beam).

1335 $cm^{-1}$) species spectra were then integrated versus time. Their chemigrams are represented in Fig. 6, together with the evolution profiles of the representative gas phases detected by mass spectrometry [$^{12}CO_2$ ($m/z$ = 44), $^{13}CO_2$ ($m/z$ = 45), $^{12}CH_3OH$ ($m/z$ = 29, to avoid interferences with oxygen signal) and $^{13}CH_3OH$ ($m/z$ = 33); the $m/z$ intensities reported here are corrected to take into account the contribution of all species]. A delay between the exchange of half the methoxys and the detection of an equimolar mixture of gaseous natural $CH_3OH$ and $^{13}CH_3OH$ is observed at any tested temperature. This phenomenon is expected to occur with a surface whose adsorption equilibrium has been reached, since upon adsorption of a 'natural' methoxy, a $^{13}CH_3OH$ is released in the gas phase thus delaying the decrease of the $^{13}CH_3OH$ partial pressure associated to the valve switch. Furthermore, the delay between methoxy and formate formation/substitution (the more evident, the lower the reaction temperature) clearly confirms their respective position in the reaction pathway. Additionally, the perfect correlation between the formate disappearance and the carbon dioxide production nicely confirms the formate decomposition as the rate determining step of the methanol oxidation over $Au/CeO_2$, since it is possible now writing: $r_m = F_{CH_3OH} df/dw_c = dF_{CO_2}/dw_c = k_4$ [*Ce_HCOO_Au*].

One could argue that only a minor part of formate species might be intermediates. This statement can be immediately discarded observing that the totality of formates is replaced at the same rate. In the presence of both intermediate and spectator species, the fraction belonging to spectators should remain non-exchanged or exchanged at a different rate, but this was not the case. Finally, the fact that whatever the reaction temperature, the formate evolution properly parallels the $CO_2$ evolution indicates that this trend is not fortuitous.

### 3.4.3. Determining kinetic constants from SSITKA

Both the methoxy and the formate exchange curves apparently show a first order decay (i.e. exponential curve) and thus the determination of the corresponding pseudo-first-order rate constant was obtained from the slope of the linear evolution obtained when plotting Ln(relative concentration) versus time, as illustrated on Fig. 7 in the case of methoxys at 305 K. The Table 1 summarizes the rate constants obtained for both the methoxy and formate exchanges for the three tested reaction temperatures. As reported above, the formates follow the $CO_2$ evolution in the whole range of temperatures and contrarily to what was previously observed in the frame of WGS over $Pt/CeO_2$ [24], one cannot here argue that formates change from unimportant surface intermediate to potential main intermediate upon a temperature increase. As a consequence, formates being always involved in the same reaction elemental step, it is possible to determine the corresponding activation energy. Fig. 8 represents the Arrhenius plot for both formate decomposition and methoxy exchange. In both cases the linear evolution enabled to confidently estimate the activation energy and the pre-exponential factor for each of these reaction steps. The obtained data are summarized in Table 1. Emphasis should be put on the fact that the rate constant for the methoxys exchange is

**Table 1**
Kinetic data extracted from the SSITKA experiments. The values for formate oxidation to $CO_2$ were obtained either from the formate (a) or $CO_2$ (b) data.

| $T$ (K) | Methoxy exchange | | Formates to $CO_2$ | |
|---|---|---|---|---|
| | $k$/$min^{-1}$ | $E_a$ $CH_3OH \rightarrow$ Methoxy (kJ $mol^{-1}$) | $k_4$/$min^{-1}$ | $E_a$ formate $\rightarrow$ $CO_2$ (kJ $mol^{-1}$) |
| 344 | 1.58E−01 | 7.9 | 6.56E−02 (a)<br>6.70E−02 (b) | 38.0 (a)<br>39.2 (b) |
| 316 | 1.19E−01 | $A$ ($min^{-1}$)<br>2.49E+00 | 1.42E−02 (a)<br>1.75E−02 (b) | $A$ ($min^{-1}$)<br>3.54E+04 (a)<br>5.81E+04 (b) |
| 305 | 1.14E−01 | | 1.33E−02 (a)<br>1.21E−02 (b) | |

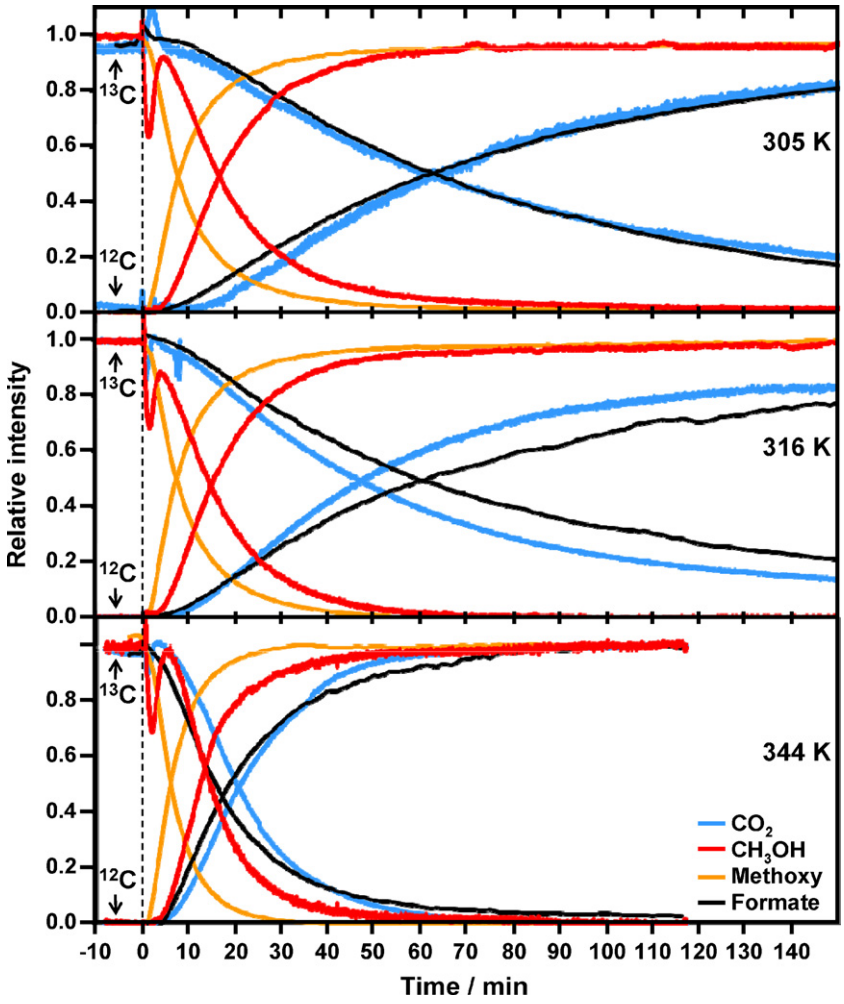


**Fig. 6.** Methanol oxidation over Au/$CeO_2$: as set of SSITKA experiments realized at various temperatures. The curves represent the chemigrams relative to the main observed species when a switch from $^{13}CH_3OH$ to $^{12}CH_3OH$ (at $t = 0$) was made.

higher than that corresponding to formate decomposition, essentially due to a much lower activation energy. Such a low activation energy (7.9 kJ $mol^{-1}$) is consistent with the following equilibrium taking place:

$$^{12}CH_3OH + {}^{13}CH_3O\_Ce* = {}^{13}CH_3OH + {}^{12}CH_3O\_Ce*$$

In fact, if the following reaction:

$$^{13}CH_3O\_Ce* + *Au\_O_2 \rightarrow *Ce\_H{}^{13}COO\_Au* + H_2O$$

was the main contribution to the $^{13}CH_3O\_Ce^*$ decay, the methoxys and formate curves should not be delayed.

Finally, the SSITKA method possesses the great advantage to enable the determination of the activation energy of an elemental reaction step. Consequently, the activation energy for the formate decomposition proposed as the rate determining step was determined with a value of $E^a_{RDS} = 39.2$ kJ$mol^{-1}$. This value of $E^a_{RDS}$ should now be compared to the apparent activation energy determined from the gas phase data: $E^a_{app} = 27.6$ kJ$mol^{-1}$. In agreement with what was deduced from the kinetic model, the apparent activation energy is lower than the activation energy required for the RDS. According to the different hypotheses, two possibilities can be expected here, either $E^a_{app} = E^a_{RDS} + \Delta H_3$ or $E^a_{app} = E^a_{RDS} + \Delta H_3 + \Delta H_1$, where the $\Delta H_1$ value refers to the $O_2$ adsorption heat onto gold (which is expected to be quite low taking into account the low affinity of gold for oxygen [25]), while $\Delta H_3$ corresponds to the enthalpy relative to the exothermic oxidation of methoxys into formates in the adsorbed state (difficult to estimate). Moreover, it is worth emphasizing that the low value for $E^a_{app} - E^a_{RDS} = -11.6$ kJ$mol^{-1}$ is consistent with the absence of $\Delta H_2$ (methanol adsorption heat) in the expression of the apparent activation energy and thus with the zero partial order for methanol. Literature reports values for alcohol adsorption heat on metal oxides ranging from to −55 to −130 kJ $mol^{-1}$, indeed [26–30].

### 3.5. The remaining problem of the "active perimeter"

To explain the necessity to have a quasi total surface coverage before formate formation and thus $CO_2$ production [9], the presence of an active perimeter around the metal particles [31], i.e. a zone at the interface between the gold clusters and the oxide support where the adsorbed species (in this case the formates) are formed and transformed, was invoked. In the present paper, the kinetic model which was developed is consistent with the experimental data indicating the absence of formates over gold free ceria, in the tested low temperature range [9]. Indeed, the third step of our kinetic model directly involves gold for the methoxy transformation into formates, at the boundary between gold and ceria. However, this assumption may be too simple and one cannot exclude that activated oxygen species diffuse towards methoxys through surface vacancies within a region defined by its active perimeter. Only this region would be active for both formate formation and their further decomposition. So, in the proposed reaction

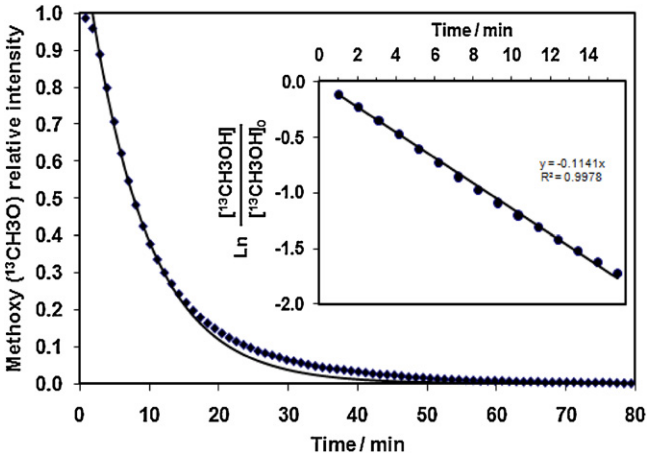


**Fig. 7.** Evaluation of the kinetic constant relative to $^{13}$C-methoxy replacement by $^{12}$C-methoxy during the steady state methanol oxidation over Au/$CeO_2$ at 305 K. The inset shows the typical plot for an order one reaction rate while (♦) stands for the SSITKA experimental data and (—) for the corresponding theoretical plot.

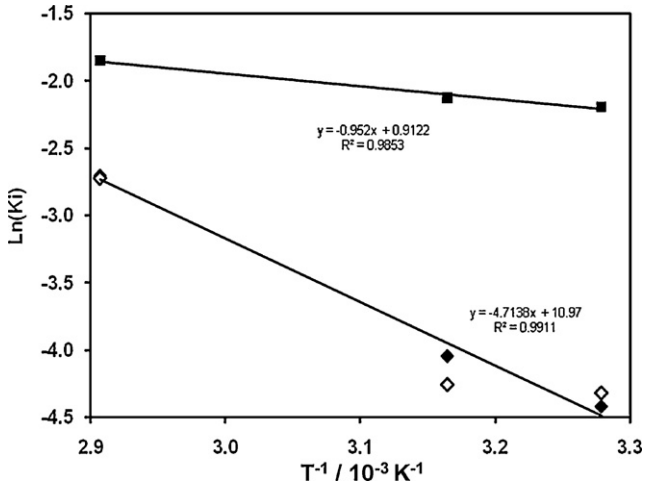


**Fig. 8.** Arrhenius plots for the determination of activation energies relative to elemental steps occurring in the methanol oxidation: methoxy exchange (■) and formate decomposition to $CO_2$ from formate (◊) and $CO_2$ (♦) evolutions.

model, methanol is dissociatively adsorbed on the oxide surface; linear and bridged methoxys transform into formates in a region defined as the active perimeter; those formates which are close enough to the gold particles decompose to give rise to adsorbed CO, which is finally oxidized on the gold nanoclusters. Being the formate decomposition the rate determining step, the formates and thus methoxys are "queuing" at the limit of the active perimeter, waiting for a place where to transfer and react. Therefore, the limiting factor for carbon dioxide production would be the number and the extent of such regions. Their number is obviously related to metal loading and dispersion: for our 1 wt% loading sample, gold area was calculated to be $A_{Au} = 0.86\ m^2\ g_{cat}{}^{-1}$, therefore having the catalyst 180 $m^2\ g^{-1}$ surface area, the concentration of such clusters is ≤0.5% of the $CeO_2$ surface [32]. However, estimating the extent of such active perimeter regions is less obvious and the assistance of theoretical calculations would be greatly helpful.

## 4. Conclusions

The present paper aimed at clarifying the mechanism of methanol full oxidation over Au/$CeO_2$ in the low temperature range. A more kinetic approach was applied when compared to our previous paper confirming a quite low value for the apparent activation energy. This low activation energy implies an initiation of the reaction at low temperature and thus the conversion oscillations that were observed during the *operando* analysis of the catalyst were related to local heating effects arising from the IR irradiation of the sample. The kinetic approach also allowed us to determine a zero partial order for methanol which must be associated to a high catalyst surface coverage under chemical steady state, the oxide surface being almost full of methoxys when the formate formation initiates.

A global kinetic modeling of the reaction which takes into account all the experimental data and assumes the formate decomposition as the rate determining step was then proposed. Thanks to the SSITKA experiments, further evidences were found for the formate decomposition being the rate determining step. Indeed, the rate for the formate decomposition and the $CO_2$ production were found similar at three distinct reaction temperatures. The SSITKA experiments also allowed to determine the activation energy associated to the RDS. The obtained value is somewhat lower than the apparent activation energy and the difference between the values is consistent with the proposed kinetic model. Finally, even if the developed model is consistent with the experimental data, one must admit that the elemental sequences chosen for the kinetic modeling of the reaction could be too simple. For example, in order to take into account the noticeable amount of adsorbed reactive formates under steady-state conditions, the existence of an active parameter around the gold nanoparticles is highly probable, even if up to now the extent of these active regions is not available.

## Acknowledgement

Rhodia company is kindly acknowledged for having provided the sample used for this study.

## References

[1] C. Jia, S. Batterman, C. Godwin, S. Charles, J.-Y. Chin, Indoor Air 20 (2010) 357–369.
[2] M. Ongwandee, R. Moonrinta, S. Panyametheekul, C. Tangbanluekal, G. Morrison, Build. Environ. 46 (2011) 1512–1522.
[3] H. Jarnstrom, K. Saarela, P. Kalliokoski, A.L. Pasanen, Indoor Built Environ. 17 (2008) 313–323.
[4] F. Gouriou, J.-P. Morin, M.-E. Weill, Atmos. Environ. 38 (2004) 2831.
[5] M. Haruta, T. Kobayashi, H. Sano, N. Yamada, Chem. Lett. 16 (1987) 405.
[6] M. Haruta, CATTECH 6 (2002) 102.
[7] C. Louis, in: D. Astruc (Ed.), Nanoparticles and Catalysis, Wiley-VCH, Weinheim, 2008, pp. 475–503.
[8] P.Y. Sheng, G.A. Bowmaker, H. Idriss, Appl. Catal. A 261 (2004) 171.
[9] S. Rousseau, O. Marie, P. Bazin, M. Daturi, S. Verdier, V. Harlé, J. Am. Chem. Soc. 132 (2010) 10832–10841.
[10] T. Lesage, C. Verrier, P. Bazin, J. Saussey, M. Daturi, Phys. Chem. Chem. Phys. 5 (2003) 4435–4440.
[11] I. Malpartida, E. Ivanova, M. Mihaylov, K. Hadjiivanov, V. Blasin-Aubé, O. Marie, M. Daturi, Catal. Today 149 (2010) 295.
[12] S. Wuttke, P. Bazin, A. Vimont, C. Serre, J.S. Chang, G. Férey, M. Daturi, Chem. Sci., submitted for publication.
[13] M. Eiswirth, G. Ertl, Surf. Sci. 177 (1986) 90–100.
[14] K.M. Khan, Physica A 278 (2000) 526–537.
[15] M.A. Vannice, Kinetics of Catalytic Reactions, Springer, New-York, 2005.
[16] M.P. Kapoor, Y. Ichihashi, K. Kuraoka, W.J. Shen, Y. Matsumura, Catal. Lett. 88 (2003) 83.
[17] M.P. Kapoor, A. Raj, Y. Matsumura, Microporous Mesoporous Mater. 44 (2001) 565.
[18] A. Vimont, F. Thibault-Starzyk, M. Daturi, Chem. Soc. Rev. 39 (2010) 4928–4950.
[19] C. Lamberti, E. Groppo, G. Spoto, S. Bordiga, A. Zecchina, C.G. Bruce, K. Helmut, Advances in Catalysis, vol. 51, Academic Press, 2007, pp. 1–74.
[20] C. Lamberti, A. Zecchina, E. Groppo, S. Bordiga, Chem. Soc. Rev. 39 (2010) 4951.
[21] A.M. Efstathiou, X.E. Verykios, Appl. Catal. A-Gen. 151 (1997) 109–166.
[22] G.G. Olympiou, C.M. Kalamaras, C.D. Zeinalipour-Yazdi, A.M. Efstathiou, Catal. Today 127 (2007) 304–318.
[23] S. Pinchas, L. Laulicht, Infrared Spectra of Labelled Compounds, Academic Press, London and New York, 1971.
[24] F.C. Meunier, D. Tibiletti, A. Goguet, S. Shekhtman, C. Hardacre, R. Burch, Catal. Today 126 (2007) 143.
[25] http://web.mit.edu/2.813/www/readings/Ellingham_diagrams.pdf.

[26] J.D. Butler, J. Chem. Soc. B: Phys. Org. (1968) 905.
[27] F. Figueras Roca, P. Renard, L. De Mourgues, J. Chim. Phys. Phys.-Chim. Biol. 65 (1968) 1393.
[28] S. Kolboe, J. Catal. 13 (1969) 199.
[29] M.J. O'Brien, R.L. Grob, J. Chromatogr. 155 (1978) 129.
[30] P.F. Rossi, G. Busca, G. Ramis, V. Lorenzelli, J. Calor. Anal. Therm. Thermodyn. Chim. 17 (1986) 369.
[31] R. Leppelt, B. Schumacher, V. Plzak, M. Kinne, R.J. Behm, J. Catal. 244 (2006) 137–152.
[32] Supplementary information of ref. [9].